

# INVESTIGATING THE COMPARISON OF SHIP RESISTANCE COMPONENTS BETWEEN U AND V-SHAPED HULLS

Muhammad Luqman Hakim\*, Tuswan, Ahmad Firdaus, Ocid Mursid

Department of Naval Architecture, Faculty of Engineering, Universitas Diponegoro, Semarang, Indonesia 50275

## Article history

Received

17 October 2022

Received in revised form

26 March 2023

Accepted

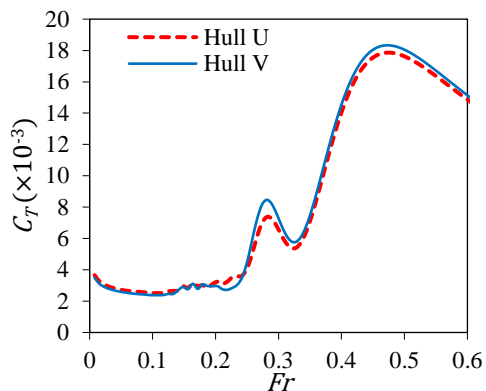
27 March 2023

Published Online

19 April 2023

\*Corresponding author  
mluqmanhak@lecturer.undip.ac.id

## Graphical abstract



## Abstract

The selection of a hull design with minimal drag is an important effort to reduce emission levels on ships. Two different hull shapes, U and V hulls, have unique properties that affect their drag production, which has been studied extensively in the past. This study aims to re-examine the differences between the two hull types by conducting a simple analysis of drag prediction results using empirical and numerical slender body methods. Both hull models in this study have the same size and volume. The results indicate that the U hull has a higher frictional resistance ( $R_f$ ) than the V hull due to its wider wetted surface area ( $WSA$ ). Additionally, the viscous pressure resistance ( $R_{vp}$ ) and form factor coefficient ( $k$ ) of the U hull are also higher than those of the V hull. However, for Froude numbers ( $Fr$ ) above 0.245, the U hull has lower wave resistance ( $R_w$ ) than the V hull, whereas for  $Fr$  below 0.245, the U hull has higher  $R_w$ . Overall, the U hull produces a higher total resistance ( $R_T$ ) than the V hull at low speeds, but a lower  $R_T$  at high speeds. Therefore, the choice of hull shape for minimizing a ship's resistance is influenced by the desired speed of service. If  $Fr$  is low, below 0.24, a V-shaped hull is more suitable. However, if  $Fr$  is higher than 0.24, a U-shaped hull is more appropriate.

Keywords: Hull shape, U hull, V hull, ship resistance, Formdata

© 2023 Penerbit UTM Press. All rights reserved

## 1.0 INTRODUCTION

Special efforts need to be made to reduce emission levels or increase the efficiency of energy use on ships. The IMO notes that by 2021, the emission level from ships worldwide reached 2.2% of the total CO<sub>2</sub> emissions created by humans [1]. If no precautions are taken, the emission level is projected to increase by 2 to 3 times [2]. Wang and Lutsey [3], as well as Molland *et al.* [4], have described several methods to increase the efficiency of energy use on ships. These methods include weather routing [5], [6], speed reduction [7],

[6], propeller [8], [9], and hull optimization [10], [11], bow modification [12], [13], [14], hull cleaning management or preventing biofouling [15], [16], [17], [18], [19], [20], trimming strategy [21], adding devices [22], [23], [24], [25], [26], using more advanced anti-fouling [27], [28], [29], and analyzing the coating roughness [30], [31], [32], [33], [34], etc.

To reduce ships' emissions, one effective method is to choose a hull shape design with minimal drag. The shape of the hull is closely tied to the type of ship and its respective duties [36]. Several studies have analyzed hull shape modifications, such as the

modification of the bulbous bow shape by Choi [37] and Kleinsorge et al. [11], the modification of hull shape by Eberechukwu et al. [10], and the work of Jung and Kim [38], Chrismianto et al. [39], and Fitriadhy et al. [40].

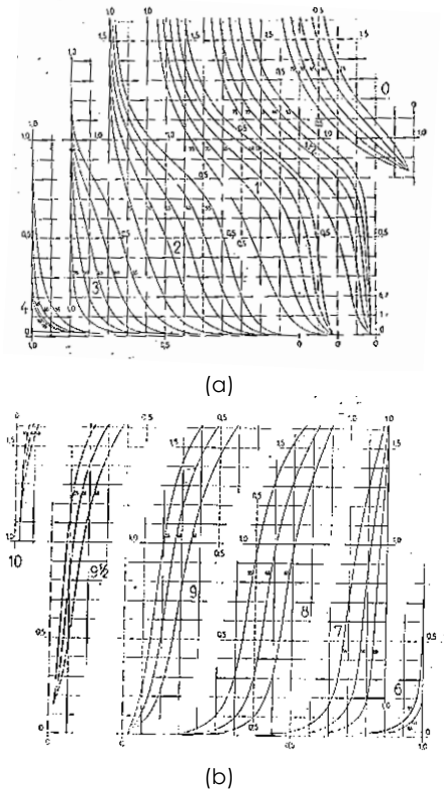


**Figure 1** Body plan for the stern (a) and bow (b) for the U hull [35]

The shape of the hull can be determined by the lines plan, which includes three forms: V, U, and N shapes, according to FORMDATA I and FORMDATA II [41][35]. Figure 1 and Figure 2 illustrate the curved lines of the body plan for the U and V hulls, respectively. While the two hulls may appear similar at first glance, a closer examination and comparison, as shown in Figure 3, reveals differences in the curvature line patterns [36]. The V hull features mostly straight lines, whereas the U hull is characterized by curves. Despite these differences, the two hulls have the same area or volume.

Different variations in hull shape have distinct characteristics that impact the designer's choice based on the ship's mission. These characteristics affect various aspects of design, hydrodynamics, construction, and production. For example, the U hull has a wider bottom area than the V hull, as seen from the design aspect [36]. From the construction aspect, the U hull has more strength than the V hull with the same structural size [42]. The V hull is easier to produce due to the lesser need for bending plates during production [43]. In terms of drag, both the U and V hulls have unique characteristics. Schneekluth &

Bertram [36] found that the U hull produces less wave resistance than the V hull for high Froude numbers.

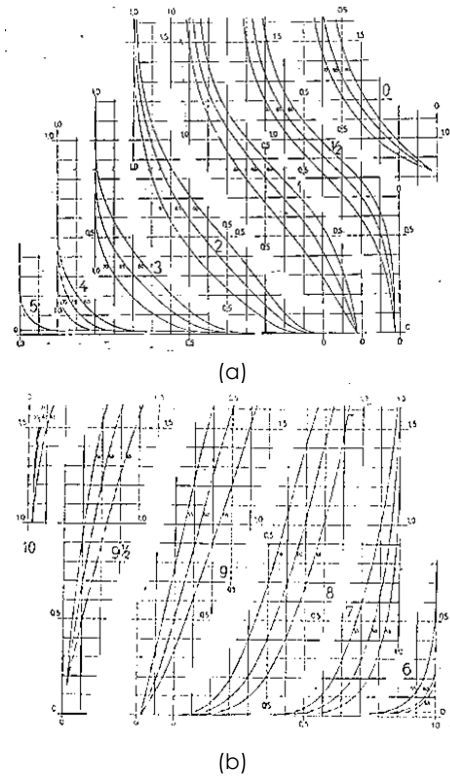


**Figure 2** Body plan for the stern (a) and bow (b) for the V hull [35]

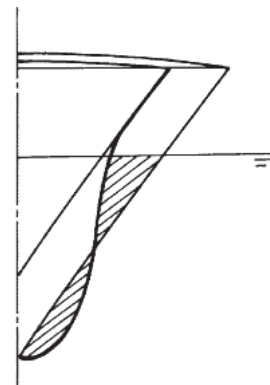


**Figure 3** The difference in the cross-sectional shape of the front U and V with the area under the same draft [36]

According to the literature, variations in hull shape only affect the wave resistance components and not the other resistance components such as frictional and viscous pressure resistance, which have not been specifically described. The total resistance of a ship is determined by adding up all these resistance components. The authors of a study suggested that differences in hull shape could also cause variations in the other resistance components. Therefore, a U-shaped hull that has lower wave resistance may not necessarily have lower total resistance.

This study aims to demonstrate the drag specificity resulting from each hull shape by investigating the differences in predicted drag values using two simple

methods: the empirical and numerical the slender body methods. To ensure a fair comparison, both the U and V hulls were constructed to have the same size and volume displacement values according to the Formdata II procedure. The Maxsurf software's student version assisted the work in this study. The analysis of the two hulls involves comparing their hydrostatic characteristics, frictional resistance, viscous pressure resistance, wave resistance, and total resistance.

## 2.0 METHODOLOGY

This chapter outlines the methodology employed in conducting a comparative analysis. The study commenced by creating line plans based on Formdata II [35], followed by a comparison of hull characteristics for both hulls. Next, drag components were calculated using both empirical and numerical techniques. Empirical methods were utilized to predict frictional resistances, viscous pressure resistance, and form factor, while the numerical method, slender body, was utilized to predict wave resistance.

### 2.1 Making Both Hull Models

The process of creating the lines plan models for the U and V hulls involved referencing Formdata II, as depicted in Figure 1 and Figure 2. The process commenced by selecting the body plan or station line shape, based on the available lines. The line selection process also accounted for the desired  $C_B$  (coefficient block) and  $L_{CB}$  (length of center buoyancy) values, which are described in Table 1 along with the values of the main dimensions for both models.

**Table 1** The main dimensions of both hull models

Item	Description	Value	Unit
$L_{PP}$	Length of Perpendicular	60	m
$L_{WL}$	Length of Waterline	62.3	m
$B$	Breadth	12	m
$H$	Depth	4	m
$T$	Draught	2.7	m
$C_B$	Coefficient Block	0.6	
$L_{CB}$	Length of center Buoyancy from midship	1.55	%

Figure 4 illustrates the difference in cross-sectional lines between the U hull and V hull models. The red lines depict the station lines for the U hull, while the blue lines represent those for the V hull. The differing characteristics of the station lines for both hulls are consistent with those shown in Figure 3. Specifically, the U hull has a larger area at the bottom than the V hull, while the V hull has a larger area at the draft than the U hull. The 3D hull models, which were created using Maxsurf software, can be viewed in Figure 5, where the U hull model is shown in red and the V hull model is shown in blue.

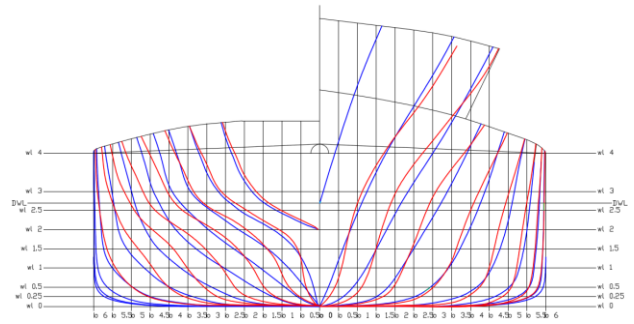


**Figure 4** Comparison of cross-sectional or body plans (stations) of the U hull (red) and V hull (blue line) models

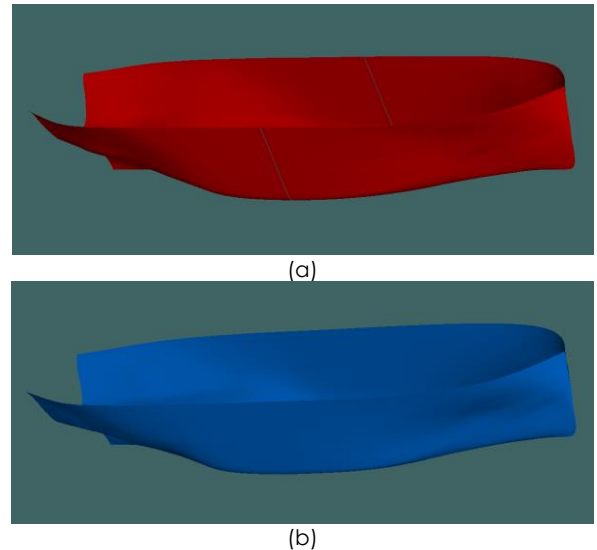


**Figure 5** 3D models of the U hull (red) and the V hull (blue)

### 2.2 Ship Resistance Components

The equation for the ship drag component is written in Equation 1 [44], where  $R_T$  is the total resistance,  $R_F$  is the frictional resistance,  $R_{VP}$  is the viscous pressure resistance,  $R_W$  is the wave resistance, and  $1 + k$  is the form factor. Generally, Equation 1 can be converted into the coefficients form shown in Equation 2, where  $C_T$  is the total resistance coefficient,  $C_F$  is the frictional resistance coefficient,  $C_{VP}$  is the viscous pressure resistance coefficient,  $C_W$  is the wave resistance coefficient. All of the coefficients are explained in Equations 3 to 5, where  $V$  is the velocity,  $\rho$  is the density of the fluid, and  $S$  is the surface area of the hull submerged in water.

$$R_T = R_F + R_{VP} + R_W = R_F(1 + k) + R_W \tag{1}$$

$$C_T = C_F + C_{VP} + C_W = C_F(1 + k) + C_W \tag{2}$$

$$C_F = \frac{R_F}{\frac{1}{2}\rho V^2 S} \tag{3}$$

$$C_{VP} = \frac{R_{VP}}{\frac{1}{2}\rho V^2 S} \tag{4}$$

$$C_W = \frac{R_W}{\frac{1}{2}\rho V^2 S} \tag{5}$$

**2.3 Empirical Methods**

The empirical methods used in this study to predict the resistance components consist of the  $C_F$  formula from ITTC 1957 [45] to estimate frictional resistance, the form factor formula from Holtrop [46] to determine the value of the viscous pressure resistance, and the wave resistance formula also from Holtrop [46].

The frictional resistance is predicted using the  $C_F$  formula from ITTC 1957 [45] shown in Equation 6. In this formula, it can be seen that the  $C_F$  value is a function of  $Re$  (Reynolds number) described in Equation 7, where  $\rho$  is the density of the fluid,  $V$  is the speed of the ship,  $L$  is the length of the ship ( $L_{WL}$ ),  $\mu$  is dynamic viscosity.

$$C_F = \frac{0.075}{(\text{Log}_{10} Re - 2)^2} \tag{6}$$

$$Re = \frac{\rho V L}{\mu} \tag{7}$$

The viscous pressure resistance is predicted using Equation 8, which is taken from Equation 2. The viscous pressure resistance ( $C_{VP}$ ) is related to the coefficient of form factor ( $1 + k$ ) of the hull. Thus, it is important to predict the form factor value, namely  $k$ . Holtrop [46] provides a formula to predict the form factor coefficient using the formula described in Equation 9. Equation 9 explains that the  $k$  is a function of the shape of the ship's stern, namely  $C_{stern}$  which values are described in Table 2. The other parameters consist of the length of the hull ( $L$ ), the breadth ( $B$ ), the draft ( $T$ ), the length of the hull at the waterline ( $L_{WL}$ ). Then,  $L_R$  is the length of run which if not known can use Equation 10, where  $C_P$  is the prismatic coefficient and  $L_{CB}$  is the length of center buoyancy position to midship.

**Table 2** Parameter value of afterbody form [46]

Afterbody form	$C_{stern}$
Pram with gondola	-25
V-shaped sections	-10
Normal section shape	0
U-shaped sections	10

$$C_{VP} = C_F k \tag{8}$$

$$k = f(C_{stern}, B, L, T, L_{WL}, L_R, \nabla, C_P) \tag{9}$$

$$L_R = f(L_{WL}, C_P, L_{CB}) \tag{10}$$

The wave resistance was also predicted using the empirical method from Holtrop [46]. The wave resistance is also predicted using the slender body numerical method described in the next subsection.

Holtrop's empirical method for predicting wave resistance is illustrated in Equation 11, where  $R_W(Fr)$  is a function of the displaced volume in  $m^3$  ( $\nabla$ ),  $L$ ,  $\rho$ , acceleration of gravity ( $g$ ),  $T$ ,  $B$ ,  $C_B$ , Froude number ( $Fr$ ), the half angle of entrance ( $i_E$ ), midship coefficient ( $C_M$ ),  $C_P$ . The half-angle of the entrance ( $i_E$ ) is described in Equation 12, where it is a function of  $L$ ,  $B$ ,  $C_{WP}$  (coefficient of water plan area),  $C_P$  and  $L_{CB}$ .

$$R_W(Fr) = f(\nabla, L, \rho, g, T, B, C_B, Fr, i_E, C_M, C_P) \tag{11}$$

$$i_E = f(L, B, C_{WP}, C_P, L_{CB}) \tag{12}$$

**2.4 Numerical Methods Slender Body**

The wave resistance was predicted using the slender body numerical method assisted by Maxsurf software. This method was first developed Michell [47], which was later enhanced by Insel and Molland [48] and Couser et al [49]. It can be seen in Figure 6, how the hull is positioned on the axis, where the x-axis points forward, y points to the right, and z points downwards. The vertical line of the tank is at  $y = 0$  and the free surface of the water is at  $z = 0$ . The hull model is discretized into rectangular panel elements, see the illustration in Figure 7. The wave resistance is calculated from the expression derived by Insel [50] which describes the drag in the form of the far-field Eggers [51] coefficient as a finite element source.

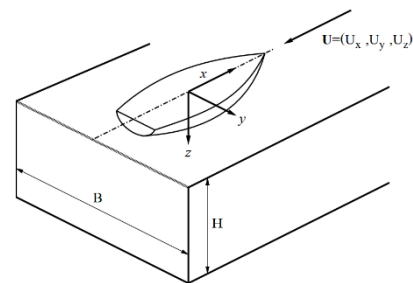


**Figure 6** Main notation and axis convention of slender body method [49]

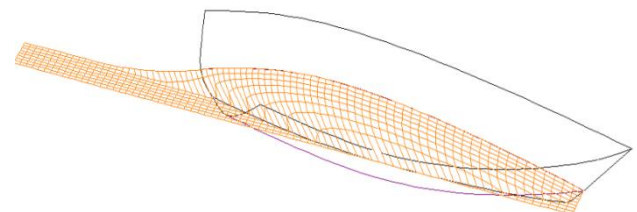


**Figure 7** Slender body mesh [55]

The slender body method can be used if the ship's hull is symmetrical and flat with a size ratio of  $L/\sqrt[3]{\nabla} > 4$  [52], [53], [54]. For these hull models used, based on the main size values in Table 1, the value of  $L/\sqrt[3]{\nabla}$  is 5.845. So that the slender body method can be used for the size of these two hull models.

### 2.5 Validation

In this study, the slender body method, which was simulated using Maxsurf, was validated against the work done by Bašić et al. [56]. The hull model used in the validation process is similar to the one used by Bašić et al. [56], namely Series 60 without a bulb, with dimensions of  $L_{pp} = 3.0$  m,  $B = 0.40$  m,  $T = 0.163$  m, and  $C_B = 0.6$ . The Series 60 model is part of the reference model library on Maxsurf. The results obtained from the slender body method were compared to the results from the original thin-ship theory, the modified thin-ship theory, and the CFD simulation conducted by Bašić et al. [56], as well as experimental results from Toda et al. [57].

The validation results are presented in

Figure 8. Although there is some deviation between the results at  $0.25 < Fr < 0.35$ , the other results are very close. Based on these findings, the authors believe it is appropriate to proceed to the specimen model simulation stage, as the purpose of this simulation is solely to compare the U and V shapes with other parameters held constant.

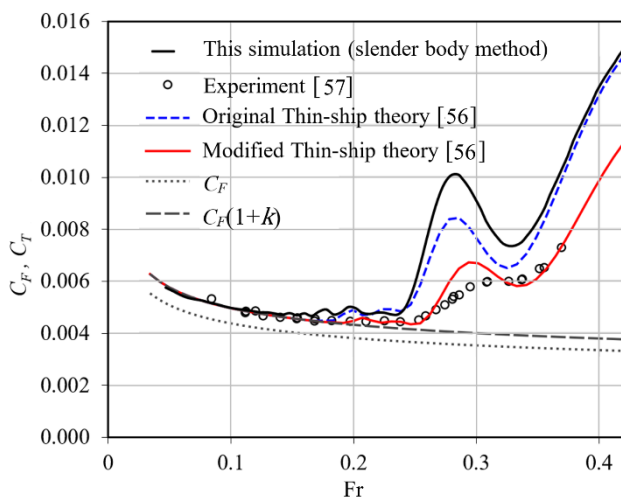


Figure 8 Validation results

## 3.0 RESULTS AND DISCUSSION

### 3.1 Differences in hydrostatic characteristics

After obtaining the body plan for the U and V hulls using the Formdata method, both hulls were modelled in 3D using Maxsurf software. The software was used to calculate and compare the hydrostatic characteristics of both hulls. The results of these calculations are presented in Table 3. To aid in comparative analysis, Equation 13 was used for this and subsequent comparisons.

Comparing the U and V shapes of two hulls, certain parameters must be the same, while others must be different to determine the differences in shape. The parameters that must be the same include  $L$  (length),  $B$  (breadth),  $T$  (draft),  $C_B$  (block coefficient),  $C_P$

(prismatic coefficient),  $C_M$  (midship coefficient),  $L_{CB}$  (longitudinal center of buoyancy), and  $L_{CF}$  (longitudinal center of flotation). These parameters are not affected by differences in the shape of the hulls. On the other hand, the parameters that must be different include  $WSA$  (wetted surface area),  $C_{WP}$  (coefficient of wave profile), and  $K_B$  (block coefficient). These parameters will obviously differ between the two hulls. By comparing the U and V shapes of the two hulls while controlling for these parameters, we can better understand the impact of differences in shape.

Based on the calculation results shown in Table 3, it can be observed that there is a very slight difference in the volume displacement value between hull U and hull V, which is only  $0.2 \text{ m}^3$  or  $0.02\%$ . This difference can be considered negligible since it is a result of the precision in the model creation. The values of  $L$ ,  $B$ ,  $T$ , and  $C_B$  for both models are also identical. Parameters  $C_P$ ,  $C_M$ ,  $L_{CB}$ , and  $L_{CF}$  have minimal differences, which are less than  $0.3\%$ . Due to these small differences, it is reasonable to assume that both hulls share similar values for certain parameters, allowing for proper analysis of the comparative drag value.

$$\Delta\% = \frac{\text{result of U} - \text{result of V}}{\text{result of V}} \times 100\% \quad (13)$$

Table 3 Results of the differences in hydrostatic characteristics of the U and V hulls

Parameter	Units	Value		$\Delta\%$
		U hull	V hull	
Volume disp.	$\text{m}^3$	1188.40	1188.20	0.017
$L_{WL}$ ( $L$ )	m	62.306	62.306	0.000
Breadth ( $B$ )	m	12.000	12.000	0.000
Draft ( $T$ )	m	2.700	2.700	0.000
$WSA$	$\text{m}^2$	735.331	726.387	1.231
$C_B$		0.586	0.586	0.000
$C_P$		0.600	0.600	0.000
$C_M$		0.979	0.979	0.000
$C_{WP}$		0.703	0.705	-0.284
$L_{CB}$ (from	%	1.548	1.549	-0.084
$L_{CF}$ (from	%	4.403	4.402	0.011
$K_B$	m	1.442	1.458	-1.097

The values that differ significantly between the two hulls are the wetted surface area ( $WSA$ ),  $C_{WP}$ , and  $K_B$ . The U hull has a greater  $WSA$  compared to the V hull, as the U hull has a longer body plan line as shown in Figure 4. The V hull has a higher  $C_{WP}$  value compared to the U hull due to its wider top and narrower bottom shape. Additionally, the  $K_B$  value for the V hull is higher than that of the U hull, as the V hull has a wider top and narrower bottom area, whereas the U hull has a wider bottom area compared to the V hull.

### 3.2 Frictional Resistance

Based on Equation 3, it can be seen that there is an input parameter value of  $S$  or  $WSA$  to predict the frictional resistance ( $R_F$ ), where the  $WSA$  for the two hulls is different. It can be seen in Table 3, that the  $WSA$  value for the U hull is higher than that of the V hull, so the  $R_F$  value for the U hull is higher than that of the V hull. The difference in the  $R_F$  value for the two hulls is 1.231% constant, comparable to the difference in the  $WSA$  value. However, because the length of both models is the same, the  $C_F$  value will be the same.

### 3.3 Viscous Pressure Resistance and Form Factor

The form factor ( $k$ ) prediction is required to predict the viscous pressure resistance. The form factor was calculated using Equation 9, where the calculation results are presented in Table 4. The prediction results show the difference between the U hull and V hull is 4.94%, where the U hull has a higher value than that of the V hull. The difference in  $\Delta\%$  was calculated using Equation 13. Based on Equation 9, the parameter that causes the difference in the form factor value is the  $C_{stern}$  parameter described in Table 2, where the value is -10 for the V hull and +10 for the U hull.

**Table 4** The difference in the prediction of the form factor

	U hull	V hull	$\Delta\%$
1+k	1.223	1.165	4.94
k	0.223	0.165	34.86

The value of the viscous pressure coefficient ( $C_{VP}$ ) can be predicted based on the form factor value. Based on Equation 8, because the  $C_F$  value is the same for both hulls, then the  $C_{VP}$  is proportional to the  $k$  value. Thus, the difference in the  $C_{VP}$  is 34.86% higher for the U hull than that of the V hull. The difference in the predicted  $R_{VP}$  is using Equation 4, where there is a  $WSA$  value parameter. Because the difference in the  $WSA$  value of about 1.231% greater for the U hull than that of the V hull, then the difference in the  $R_{VP}$  values are 36.52% higher for the U hull than that of the V hull.

The form factor value in this study is limited to using empirical methods only. For more accurate prediction, towing tank experiments or CFD simulation can be used for further study.

### 3.4 Wave Resistance

The prediction of wave resistance in this study was carried out using two methods, namely the empirical method from Holtrop [46] and the numerical method, slender body [49], [50].

#### 3.4.1 Result Using the Empirical Method

In this subsection, an analysis of the differences in the predicted wave resistance ( $R_W$ ) and the wave

resistance coefficient ( $C_W$ ) between the U hull and V hull is explained using the empirical method from Holtrop, as described in Equation 11. This prediction was assisted by Maxsurf software. The calculations were inputted from a speed of 0.375 knots to 30 knots. The calculation results for both hull models are plotted in Figure 9a for  $R_W$  result and Figure 9b for  $C_W$  result.

Based on the graph plot in Figure 9a, the wave resistance ( $R_W$ ) value for the hull U and hull V is not significantly different. The  $R_W$  for both increases as the velocity value increases. To see the difference, a comparative analysis was carried out using Equation 13, and then the comparison is plotted in Figure 10a. It can be seen in the graph that the difference between the two hulls is not significant, only in the range of -4% to 1.5%. The U hull has a lower resistance value than that of the V hull at low speeds, from 4 knots to 20 knots. The U hull has a higher wave resistance value than that of the V hull, for speeds above 20 knots.

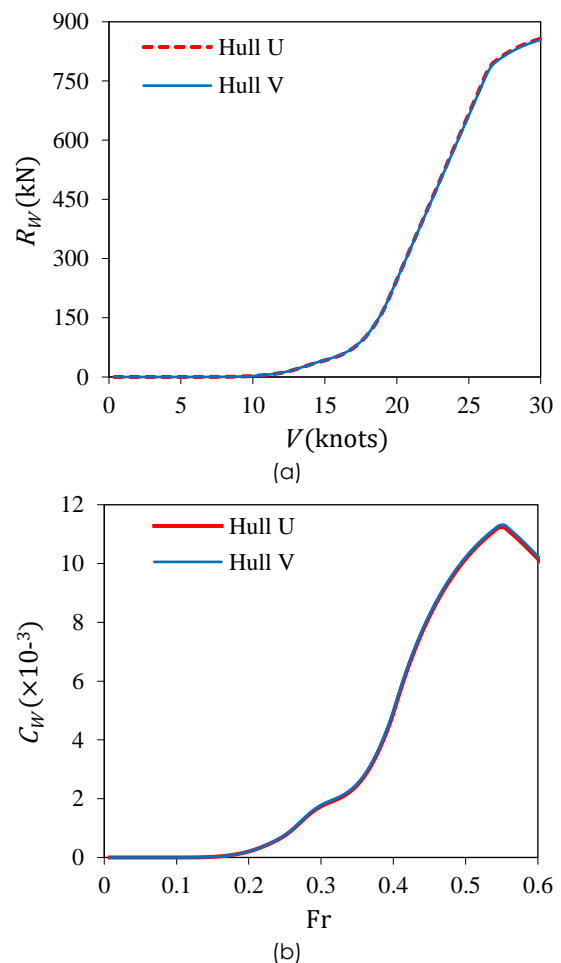


**Figure 9** The prediction of wave resistance (a) and wave resistance coefficient (b) results using the Holtrop method

The comparison of the wave resistance coefficient ( $C_W$ ) analysis with the Holtrop method for both hulls is plotted in Figure 9b and Figure 10b. It can be seen from these results that the U hull has  $C_W$  value which is

always smaller than that of the V hull from -1% to -5%, where the difference starts from the Froude number (Fr) 0.075 to 0.6.

The use of the Holtrop method for a comparative study of wave resistance for these the U hull and V hull is less visible because the parameters entered in Equation 11 and Equation 12 for both hulls have the same value, except for the  $C_{WP}$  parameter only. Therefore, the numerical slender body method was used to analyze the difference in resistance values arising from these the U hull and V hull, which is explained in the next subsection.

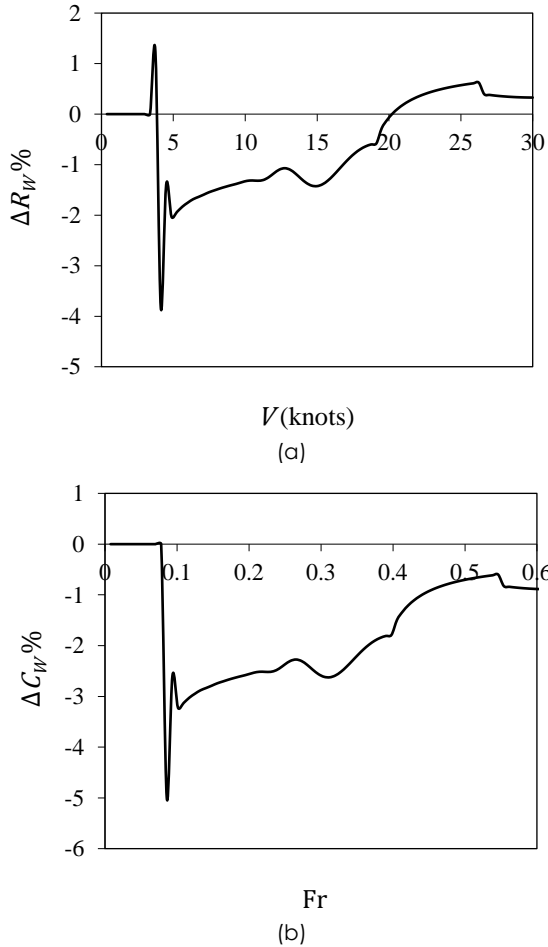


**Figure 10** The difference between the wave resistance values (a) and the wave resistance coefficient (b) for the U hull and V hull using the Holtrop method

There are disparities in the comparison outcomes between the two hull shapes shown in Figures 10a and 10b. The  $R_w$  comparison value fluctuates in Figure 10a, whereas in Figure 10b, the  $C_w$  value of U is consistently lower than that of V. It is important to note that the coefficient value is a non-dimensional value that represents the ratio of drag force to kinetic force, as explained in Equations 3, 4, and 5. Therefore, it is highly possible for these differences to arise. For example, the value of the frictional resistance coefficient

continuously decreases with increasing speed, but in reality, the resistance value still increases instead of decreasing.

**3.4.2 Result Using Slender Body Method**

The simulation results using the slender body method to analyze the difference in the wave resistance of the U hull and V hull are described in this section. The numerical calculation was assisted by Maxsurf software with input speeds between 0.375 knots to 30 knots or Froude number 0.01 to 0.6. The calculation results are plotted in Figure 11a for the wave resistance ( $R_w$ ), and in Figure 11b for the wave resistance coefficient ( $C_w$ ). Then, the comparative analysis of simulation results for the U hull and V hull is described in Figure 12a for wave resistance and Figure 12b for wave resistance coefficient. The calculation of the different analyses also used Equation 13.

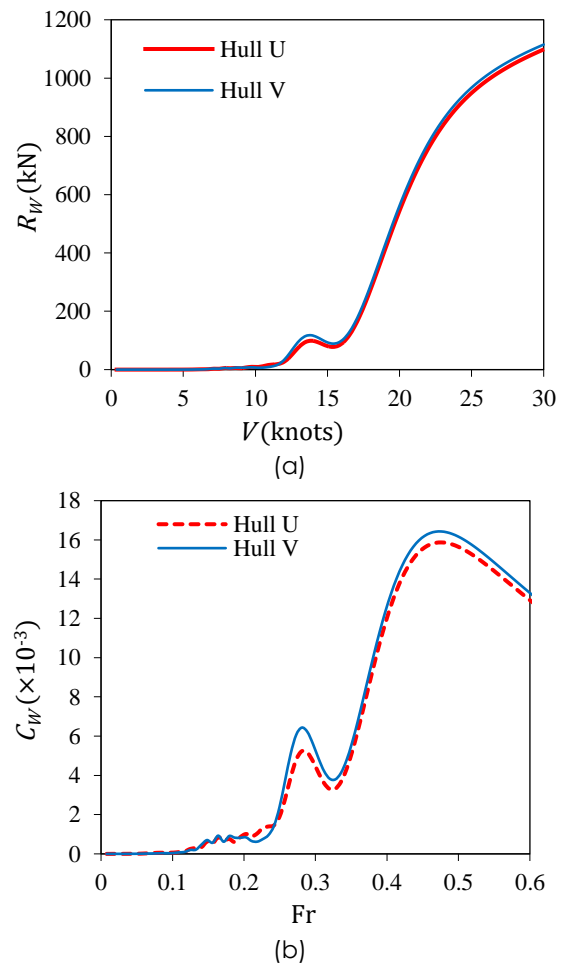


**Figure 11** The prediction of wave resistance (a) and wave resistance coefficient (b) results using slender body method

It can be seen in Figure 11a, that the prediction results of the wave resistance increase with increasing speed, but decrease and increase again at a speed of 14 knots to 16 knots. Based on these results, it can

be seen that almost overall the wave resistance for the U hull is lower than that for the V hull. Based on the results of the comparative analysis plotted in Figure 12a, the wave resistance value for the U hull is higher than that of the V hull which occurs at low speeds, from 0.375 knots to 7 knots, and from 9.5 knots to 12 knots. For high speeds, from 12 knots, the resistance of the U hull is smaller than that of the V hull. The fluctuation of the difference in the wave resistance between the two hulls is quite significant at low speeds, which is up to 120%, while for high speeds it can be up to 20%.

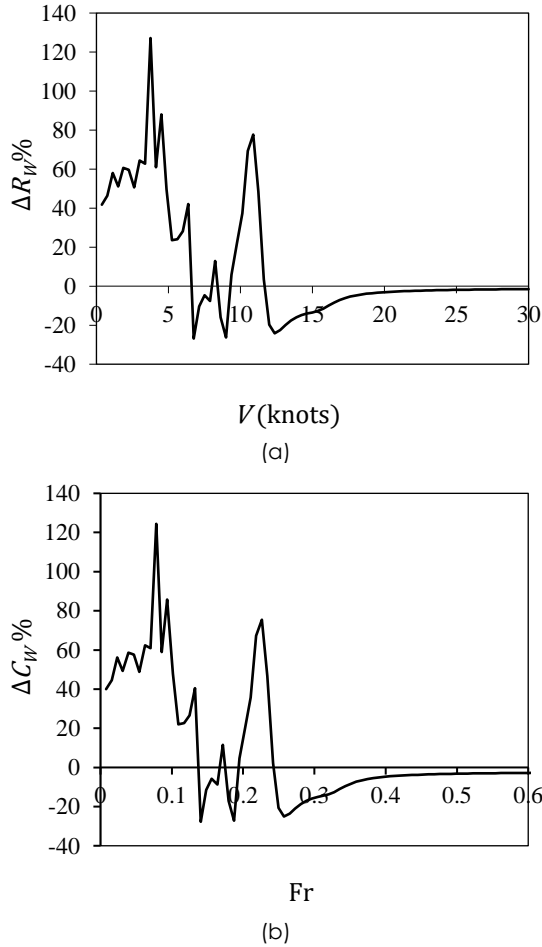


**Figure 12** The prediction of wave resistance (a) and wave resistance coefficient (b) results using slender body method

The results of calculations and comparisons in the form of wave resistance coefficients are described in Figure 11b and Figure 12b. It can be seen that the wave resistance coefficient for both hulls increased from Fr 0.01 to 0.28, then decreased from Froude number 0.28 to 0.33, and then rise again to Fr 0.47 and then decreased again. From the results of the comparative analysis plotted in Figure 12b, it shows that the value of the wave resistance coefficient for the U hull is higher than that of the V hull at the low Froude number, which is below 0.22, while at the

Froude number 0.22 and above, the U hull wave resistance coefficient value is smaller than that of the V hull.

As proof that the phenomenon of the difference in wave resistance between the U hull and V hull, the resulting wave patterns are shown in Figures 13 and 14. Figure 13 is a comparison of the wave patterns formed for the U hull (a) and V hull (b) for high speed, 13 knots (Fr 0.27). It can be seen that the wave pattern formed from the U hull has a smaller breadth and angle than that of the V hull. Meanwhile, Figure 14 is the comparison of the wave pattern formed for the U hull (a) and the V hull (b) for low speed, 4 knots (Fr 0.08). It can be seen that the wave pattern from the U hull has a wider breadth and angle than that of the V hull. Therefore, it can be concluded that the wave resistance for the U hull is higher than that of the V hull for low speeds (Fr < 0.24) and the wave resistance for the V hull is higher than that of the U hull for high speeds (Fr > 0.24).

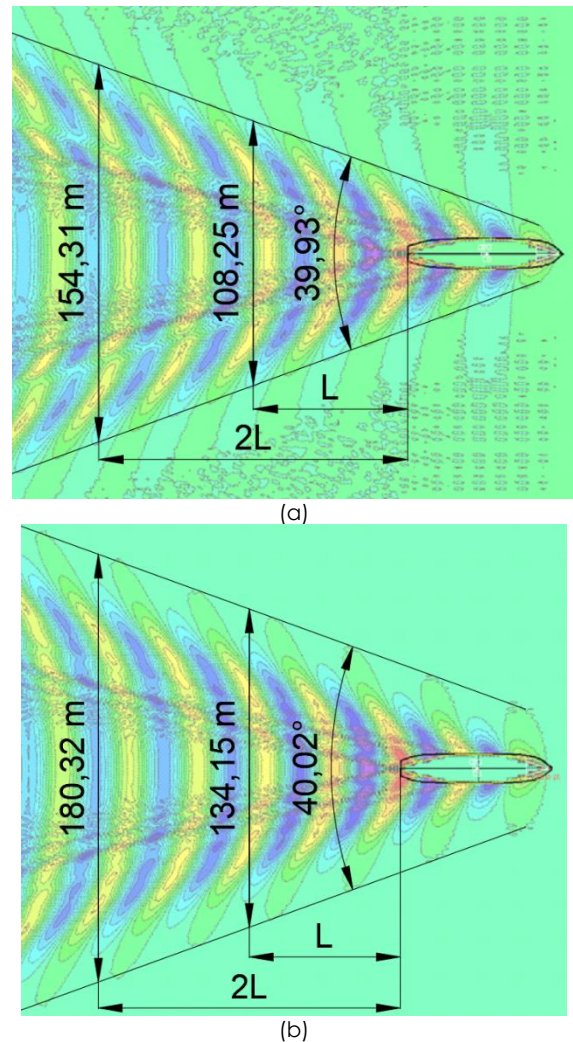


**Figure 13** The wave pattern formed of the U hull (a) and V hull (b) at a speed of 13 knots or Fr 0.27

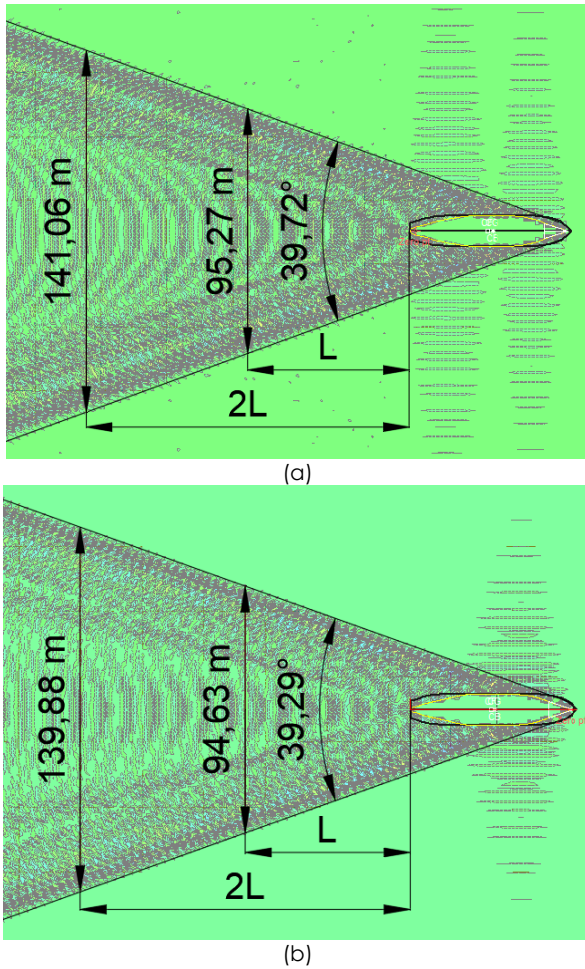


**Figure 14** The wave pattern formed of the U hull (a) and V hull (b) at a speed of 4 knots or Fr 0.08

The wave resistance value decreases and then increases again at a certain speed due to the relationship between the length of the ship and the wavelength that is formed. Wave making resistance is a type of resistance that arises due to the formation of waves by the ship's hull when moving on water. At low speeds, the waves that are formed will be larger and have higher kinetic energy, which causes the wave making resistance to increase as the ship's speed increases. However, at the critical speed, the wavelength generated by the hull will be proportional to the length of the hull itself. When this happens, the waves generated will interfere with other waves and form wave patterns that can reduce the kinetic energy of the waves generated by the ship. It is at this time that wave making resistance can decrease or even reach its minimum. The speed at which this occurs is referred to as the critical speed. After the critical speed, the waves generated by the ship will be longer and more unstable, requiring more power to produce larger waves. Therefore, the wave making resistance will increase again as the ship's speed increases.

### 3.5 Total Resistance

The total resistance calculation is the sum of the frictional, viscous pressure, and wave resistance according to Equation 1 and Equation 2. The results of the total resistance for hull U and hull V are plotted in Figure 15a, while the total resistance coefficients are plotted in Figure 15b. The wave resistance used here is the wave resistance calculated by the slender body. Meanwhile, the difference in the total drag for the U hull and V hull is plotted in Figure 16a, while the total resistance coefficients are plotted in Figure 16b. The calculation of the difference in this total resistance coefficient uses Equation 13.

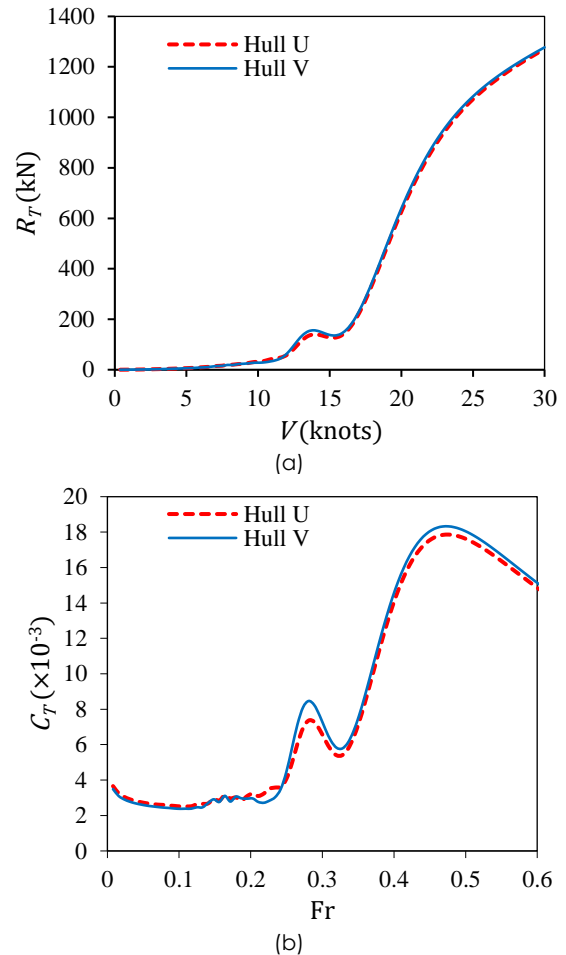


**Figure 15** The total resistances (a) and the total resistance coefficient (b) results

It can be seen in Figures 16a and 16b, that at low speeds, the Fr number is less than 0.24, and the U hull produces a higher total resistance than that of the V hull, with a different range up to 25%. As for high speed, the Fr number is more than 0.24, the U hull resulting in a total resistance smaller than that of the V hull, with a different range up to -15%.

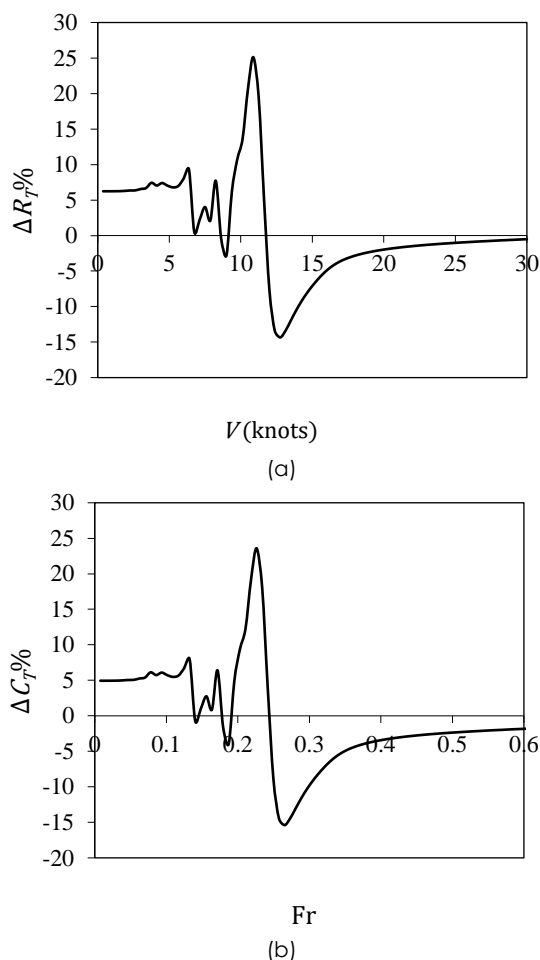


**Figure 16** The differences of the total resistance (a) and the total resistance coefficient (b)

#### 4.0 CONCLUSIONS

From the analysis results, it can be concluded that both U and V hulls have their own advantages in specific scenarios. In terms of hydrostatic differences, the two hulls show significant contrasts in  $WSA$ ,  $C_{WP}$ , and  $K_B$ . The U hull has a wider  $WSA$  than the V hull, while the  $C_{WP}$  and  $K_B$  values of the V hull are greater than those of the U hull. Additionally, the V hull has a broader top section compared to the bottom, which is distinctly different from the wider bottom of the U hull.

The analysis of the resistance differences between the two hulls was unique. First, the wider  $WSA$  value of the U hull results in a higher friction resistance compared to the V hull. Second, the U hull has a higher form factor value, resulting in higher pressure resistance than the V hull. Lastly, the U hull produces higher wave resistance than the V hull at low speeds, i.e.,  $Fr < 0.24$ , but the opposite occurs at high speeds, i.e.,  $Fr > 0.24$ , where the V hull's wave resistance is higher. However, it is important to note that this study is only applicable to displacement-type ships and not semi-displacement or planning hulls. Further research,

including towing tank experiments or computational fluid dynamics, is necessary to confirm these findings.

#### Conflicts of Interest

The author(s) declare(s) that there is no conflict of interest regarding the publication of this paper.

#### Acknowledgement

This research project was supported by the hydrodynamic laboratory Department of Naval Architecture, Faculty of Engineering, Universitas Diponegoro.

#### References

- [1] Smith, T.W.P., Jalkanen, J.P., Anderson, B.A., Corbett, J.J., Faber, J., Hanayama, S., O'Keeffe, E., Parker, S., Johansson, L., Aldous, L., Raucci, C., Traut, M., Ettinger, S., Nelissen, D., Lee, D.S., Ng, S., Agrawal, A., Winebrake, J.J., Hoen, M., Chesworth, S., Pandey, A. 2014. *Third IMO GHG Study 2014*. International Maritime Organization (IMO) London, UK. <https://doi.org/10.1017/CBO9781107415324.004>.
- [2] Buhaug, Ø., Corbett, J., Endresen, Ø., Eyring, V., Faber, J., Hanayama, S., Lee, D., Lee, D., Lindstad, H., Markowska, A., Mjelde, A., Nelissen, D., Nilsen, J., Pålsson, C., Winebrake, J., Wu, W., Yoshida, K. 2009. *Second IMO GHG Study 2009*. International Maritime Organization (IMO). <https://doi.org/10.1163/187529988X00184>.
- [3] Wang, H., Lutsey, N. 2014. Long-term Potential to Reduce Emissions from International Shipping by Adoption of Best Energy-efficiency Practices. *Transportation Research Record* 2426. 1-10. <https://doi.org/10.3141/2426-01>.
- [4] Molland, A. F., Turnock, S. R., Hudson, D. A., Utama, I. K. A. P. 2014. Reducing Ship Emissions: A Review of Potential Practical Improvements in the Propulsive Efficiency of Future Ships. *Transactions of the Royal Institution of Naval Architects Part A: International Journal of Maritime Engineering*. 156: 175-188. <https://doi.org/10.3940/rina.ijme.2014.a2.289>.
- [5] Zis, T. P. V., Psaraffis, H. N., Ding, L. 2020. Ship Weather Routing: A Taxonomy and Survey. *Ocean Engineering*. 213: 107697. <https://doi.org/10.1016/j.oceaneng.2020.107697>.
- [6] Taskar, B., Andersen, P. 2020. Benefit of Speed Reduction for Ships in Different Weather Conditions. *Transportation Research Part D: Transport and Environment*. 85: 102337. <https://doi.org/10.1016/j.trd.2020.102337>.
- [7] Leaper, R. 2019. The Role of Slower Vessel Speeds in Reducing Greenhouse Gas Emissions, Underwater Noise and Collision Risk to Whales. *Frontiers in Marine Science*. 6. <https://doi.org/10.3389/fmars.2019.00505>.
- [8] Abar, I. A. C., Utama, I. K. A. P. 2019. Effect of the Incline Angle of Propeller Boss Cap Fins (PBCF) on Ship Propeller Performance. *International Journal of Technology*. 10: 1056. <https://doi.org/10.14716/ijtech.v10i5.2256>.
- [9] Arifin, M. D., Felayati, M. F., Muhammad, A. H. 2022. Flow Separation Evaluation on Tubercle Ship Propeller. *CFD Letters*. 14: 43-50. <https://doi.org/10.37934/cfdl.14.4.4350>.
- [10] Eberechukwu Onwuegbuchunam, D., Chimobi Ogbenna, F., Charles Ezeanya, N., Okechukwu Okeke, K. 2019. Ship Hull Form Optimization: A Computational Fluid Dynamics (CFD) Approach. *International Journal of Transportation Engineering and Technology*. 5: 43. <https://doi.org/10.11648/j.ijtet.20190503.11>.
- [11] Kleinsorge, E., Lindner, H., Wagner, J., Bronsart, R. 2016. Ship

- Hull form Optimization using Scenario Methods. *PRADS 2016 - Proceedings of the 13th International Symposium on PRACTICAL Design of Ships and Other Floating Structures*.
- [12] Sugianto, E., Chen, J.-H., Permadi, N. V. A. 2022. Effect of Monohull Type and Catamaran Hull Type on Ocean Waste Collection Behavior Using OpenFOAM. *Water*. 14: 2623. <https://doi.org/10.3390/w14172623>.
- [13] Sugianto, E., Winarno, A., Indriyani, R., Horng Chen, J. 2021b. Hull Number Effect in Ship Using Conveyor on Ocean Waste Collection. *Kapal: Jurnal Ilmu Pengetahuan dan Teknologi Kelautan*. 18: 128-139. <https://doi.org/10.14710/kapal.v18i3.40744>.
- [14] Sugianto, E., Horng-Chen, J., Purba, N. P. 2021a. Numerical Investigation of Conveyor Wing Shape Type Effect on Ocean Waste Collection Behavior. *E3S Web of Conferences*. 324: 01005. <https://doi.org/10.1051/e3sconf/202132401005>.
- [15] Farkas, A., Degiuli, N., Martić, I. 2021a. Assessment of the Effect of Biofilm on the Ship Hydrodynamic Performance by Performance Prediction Method. *International Journal of Naval Architecture and Ocean Engineering*. 13: 102-114. <https://doi.org/10.1016/j.ijnaoe.2020.12.005>.
- [16] Degiuli, N., Farkas, A., Martić, I., Griž, C. G. 2023. Optimization of Maintenance Schedule for Containerships Sailing in the Adriatic Sea. *Journal of Marine Science and Engineering*. 11: 201. <https://doi.org/10.3390/jmse11010201>.
- [17] Hakim, M. L., Suastika, I. K., Utama, I. K. A. P. 2023. A Practical Empirical Formula for the Calculation of Ship Added Friction-resistance Due to (bio)fouling. *Ocean Engineering*. 271: 113744. <https://doi.org/10.1016/j.oceaneng.2023.113744>.
- [18] Hakim, M. L., Nugroho, B., Suastika, I. K., Utama, I. K. A. P. 2021. Alternative Empirical Formula for Predicting the Frictional Drag Penalty due to Fouling on the Ship Hull using the Design of Experiments (DOE) Method. *International Journal of Technology*. 12: 829. <https://doi.org/10.14716/ijtech.v12i4.4692>.
- [19] Schultz, M. P., Bendick, J. A., Holm, E. R., Hertel, W. M. 2011. Economic Impact of Biofouling on a Naval Surface Ship. *Biofouling*. 27: 87-98. <https://doi.org/10.1080/08927014.2010.542809>.
- [20] Hakim, M. L., Nugroho, B., Putranto, T., Suastika, K., Utama, I. K. A. P. 2018. Assessment of Drag Penalty Resulting from The Roughness of Freshly Cleaned and Painted Ship-Hull Using Computational Fluid Dynamics. *11st International Conference on Marine Technology MARTEC 2018*. Kuala Lumpur, Malaysia.
- [21] Undap, R., Fadillah, A. 2021. The Effect of Trim on Tanker, Container and Bulk Carrier Ship Toward the Reduction of Ship's Exhaust Gas Emission. *Kapal: Jurnal Ilmu Pengetahuan dan Teknologi Kelautan*. 18: 58-68. <https://doi.org/10.14710/kapal.v18i2.33877>.
- [22] Ismail, I. N., Manik, P., Indriyanto, M. 2020. Effect of the Addition of Hydrofoil on Lift Force and Resistance in 60 M High-Speed Vessel. *Kapal: Jurnal Ilmu Pengetahuan dan Teknologi Kelautan*. 17: 95-106. <https://doi.org/10.14710/kapal.v17i3.28772>.
- [23] Chrismiando, D., Tuswan, Manik, P. 2018. Analysis of Resistance and Effective Wake Friction Due to Addition of Stern Tunnels on Passenger Ship Using Cfd. *IOP Conference Series: Earth and Environmental Science*. 135: 012008. <https://doi.org/10.1088/1755-1315/135/1/012008>.
- [24] Samuel, S., Mursid, O., Yulianti, S., Kiryanto, Iqbal, M. 2022. Evaluation of Interceptor Design to Reduce Drag on Planing Hull. *Brodogradnja*. 73: 93-110. <https://doi.org/10.21278/brod73306>.
- [25] Adietya, B. A., Utama, I. K. A. P., Aryawan, W. D., Sutiyo, S. 2022. CFD Analysis into the Effect of using Propeller Boss Cap Fins (PBCF) on Open and Ducted Propellers, Case Study with Propeller B-Series and Kaplan-Series. *CFD Letters*. 14: 32-42. <https://doi.org/10.37934/cfdl.14.4.3242>.
- [26] Gaggero, S., Martinelli, M. 2022. Pre- and Post-swirl Fins Design for Improved Propulsive Performances. *Ship Technology Research*. 69: 31-49. <https://doi.org/10.1080/09377255.2021.1934362>.
- [27] Suwasono, B., Putra, I. K. A. S., Kristiyono, T. A., Azhar, A. 2021. Adhesive Coating Value based on the Main Ingredient of Ship Paint. *Brodogradnja*. <https://doi.org/10.21278/brod72202>.
- [28] Hakim, M. L., Nugroho, B., Nurrohman, M. N., Suastika, I. K., Utama, I. K. A. P. 2019. Investigation of Fuel Consumption on an Operating Ship due to Biofouling Growth and Quality of Anti-fouling coating. *IOP Conference Series: Earth and Environmental Science*. 339: 012037. <https://doi.org/10.1088/1755-1315/339/1/012037>.
- [29] Farkas, A., Degiuli, N., Martić, I., Vujanović, M. 2021b. Greenhouse Gas Emissions Reduction Potential by using Antifouling Coatings in a Maritime Transport Industry. *Journal of Cleaner Production*. <https://doi.org/10.1016/j.jclepro.2021.126428>.
- [30] Schultz, M. P. 2007. Effects of Coating Roughness and Biofouling on Ship Resistance and Powering. *Biofouling*. 23: 331-341. <https://doi.org/10.1080/08927010701461974>.
- [31] Atencio, B. N., Chernoray, V. 2019. A Resolved RANS CFD Approach for Drag Characterization of Antifouling Paints. *Ocean Engineering*. 171: 519-532. <https://doi.org/10.1016/j.oceaneng.2018.11.022>.
- [32] Utama, I. K. A. P., Nugroho, B., Yusuf, M., Prasetyo, F. A., Hakim, M. L., Suastika, I. K., Ganapathisubramani, B., Hutchins, N., Monty, J. P. 2021. The Effect of Cleaning and Repainting on the Ship Drag Penalty. *Biofouling*. 37: 372-386. <https://doi.org/10.1080/08927014.2021.1914599>.
- [33] Hakim, M. L., Nugroho, B., Chin, R. C., Putranto, T., Suastika, I. K., Pria Utama, I. K. A. 2020. Drag Penalty Causing from the Roughness of Recently Cleaned and Painted Ship Hull Using RANS CFD. *CFD Letters*. 12: 78-88. <https://doi.org/10.37934/cfdl.12.3.7888>.
- [34] Hakim, M. L., Maqbulyani, N., Nugroho, B., Suastika, I. K., Utama, I. K. A. P. 2021. Wind-Tunnel Experiments and CFD Simulations to Study the Increase in Ship Resistance Components due to Roughness. *Journal Of Sustainability Science And Management*. 16: 144-163. <https://doi.org/10.46754/jssm.2021.04.012>.
- [35] Gulddammer, H. E. 1963. FORMDATA II, Hydrostatic Data for Ship Forms of Full and Finer Type Hydrostatic Data, Trimmed Conditions. *International Shipbuilding Progress*. 10: 476-509. <https://doi.org/10.3233/ISP-1963-1011202>.
- [36] Schneekloth, H., Bertram, V., 1998. *Ship Design for Efficiency and Economy*. 2nd ed. Butterworth-Heinemann, Oxford.
- [37] Choi, H. J. 2015. Hull-form Optimization of a Container Ship based on Bell-shaped Modification Function. *International Journal of Naval Architecture and Ocean Engineering*. 7: 478-489. <https://doi.org/10.1515/ijnaoe-2015-0034>.
- [38] Jung, Y.-W., Kim, Y. 2019. Hull Form Optimization in the Conceptual Design Stage Considering Operational Efficiency in Waves. *Proceedings of the Institution of Mechanical Engineers, Part M: Journal of Engineering for the Maritime Environment*. 233: 745-759. <https://doi.org/10.1177/1475090218781115>.
- [39] Chrismiando, D., Manik, P., Rindo, G., Firdhaus, A. 2019. Design Comparative of PVC Fishing Boat with Variation of Ship Hullform and Fishing Gear Type. *International Journal of Mechanical Engineering and Technology*. 10: 1934-1941.
- [40] Fitriady, A., Lim, S. Y., Maimun, A. 2020. Prediction of an Optimum Total Resistance Coefficient on Catamaran using Design of Experiment (DOE) Incorporated with CFD Approach. *EPI International Journal of Engineering*. 3: 74-83. <https://doi.org/10.25042/epi-ije.022020.11>.
- [41] Gulddammer, H. E. 1962. *FORMDATA - Some Systematically Varied Ship Forms and Their Hydrostatic Data*. Copenhagen.
- [42] Hakim, M. L., Yulianto, T. 2015. Stresses Comparative Analysis Between Hull-V and Hull-U due to Slamming Pressure using Finite Element Method. *SENTA: Seminar Nasional Teori Dan Aplikasi Teknologi Kelautan*. Surabaya, Indonesia. X39-46.
- [43] Baidowi, A., Amiadji, Musriyadi, T. B., Aried, I. S., Ricinsi, F. P. 2022. Resistance Comparison of Flat Plate and

- Conventional Streamline Vessel. *IOP Conference Series: Earth and Environmental Science*.  
<https://doi.org/10.1088/1755-1315/972/1/012054>.
- [44] Molland, A. F., Turnock, S. R., Hudson, D. A. 2017. *Ship Resistance and Propulsion*. Cambridge University Press, Cambridge. <https://doi.org/10.1017/9781316494196>.
- [45] ITTC. 2014. *1978-Performance Prediction Method*. ITTC – Recommended Procedures and Guidelines 7.5-02-03-, Propulsion Committee of 27th ITTC.
- [46] Holtrop, J. 1984. Statistical Re-Analysis of Resistance and Propulsion Data. *International Shipbuilding Progress*.
- [47] Michell, J. H. 1898. XI. The Wave-resistance of a Ship. *The London, Edinburgh, and Dublin Philosophical Magazine and Journal of Science*. 45: 106-123. <https://doi.org/10.1080/14786449808621111>.
- [48] Insel, M., Molland, A. F. 1991. An Investigation into the Resistance Components of High Speed Displacement Catamarans. *Transactions*. Royal Institution of Naval Architects. 133.
- [49] Couser, P. R., Wellicome, J. F., Molland, A. F. 1998. An Improved Method for the Theoretical Prediction of the Wave Resistance of Transom-stern Hulls using a Slender Body Approach. *International Shipbuilding Progress*. 45: 331-349.
- [50] Insel, M. 1990. *An Improved Method for the Theoretical Prediction of the Wave Resistance of Transom-Stern Hulls using a Slender Body Approach*. Ph.D. Thesis, Department of Ship Science University of Southampton, U.K.
- [51] Eggers, K. 1955. Resistance Components of Two-body Ships. *Jahrbuch der Schiffbautechnischen Gesellschaft*. 49.
- [52] Jamaluddin, A., Utama, I. K. A. P., Hamdani, M. A. 2010. Kajian Interferensi Koefisien Hambatan pada Lambung Katamaran melalui Komputasi 'Slender Body Method. *Kapal Jurnal Ilmu Pengetahuan dan Teknologi Kelautan*. 7.
- [53] Gourlay, T. 2008. Slender-body Methods for Predicting Ship Squat. *Ocean Engineering*. 35: 191-200. <https://doi.org/10.1016/j.oceaneng.2007.09.001>.
- [54] Tuck, E. O. 1966. Shallow-water Flows Past Slender Bodies. *Journal of Fluid Mechanics*. 26: 81. <https://doi.org/10.1017/S0022112066001101>.
- [55] Bentley Systems. 2013. *User Manual for Maxsurf Modeler*.
- [56] Bašić, J., Blagojević, B., Andrun, M. 2020. Improved Estimation of Ship Wave-making Resistance. *Ocean Engineering*. 200: 107079. <https://doi.org/10.1016/j.oceaneng.2020.107079>.
- [57] Toda, Y., Stern, F., Tanaka, I., Patel, V. C. 1990. Mean-Flow Measurements in the Boundary Layer and Wake of a Series 60 CB = 0.6 Model Ship with and without Propeller. *Journal of Ship Research*. 34: 225-252. <https://doi.org/10.5957/jsr.1990.34.4.225>.